Optimization of plasmon–plasmon coupling in photorefractive layered media

K. R. Daly,[1,*] S. B. Abbott,[2] D. C. Smith,[2] and G. D'Alessandro[3]

[1]*School of Engineering Sciences, University of Southampton, Southampton, Hampshire, England, UK*
[2]*School of Physics and Astronomy, University of Southampton, Southampton, Hampshire, England, UK*
[3]*School of Mathematics, University of Southampton, Southampton, Hampshire, England, UK*
**Corresponding author: krd103@soton.ac.uk*

Received February 27, 2013; revised May 31, 2013; accepted June 3, 2013;
posted June 5, 2013 (Doc. ID 185871); published July 12, 2013

In this paper we study grating-induced plasmon–plasmon coupling in photorefractive layered media using a weak-coupling approximation. The method used is applicable to general layered structures that support both plasmonic and optical modes, such as photorefractive liquid crystal cells. The approximate equations are accurate when compared to S matrix approaches and capture the plasmon propagation at the surface of the device along with the optical modes guided by the layered geometry underneath. Analysis of the resulting model provides insight into the effect of the control parameters in this device and the means to optimize the diffraction efficiency. For example, by considering the case in which the plasmon is spectrally separated from the guided modes it is possible to determine the optimum gold thickness and grating strength required to obtain the strongest possible diffraction.

OCIS codes: (240.6680) Surface plasmons; (050.1950) Diffraction gratings; (000.3860) Mathematical methods in physics; (160.3710) Liquid crystals.
http://dx.doi.org/10.1364/JOSAB.30.002090

1. INTRODUCTION

A surface plasmon polariton (SPP) is a coupled oscillation between an electromagnetic field and the electron cloud at the surface of a metal [1]. SPPs have a wide variety of applications in both industry and academia. These include resonance sensors [2], enhanced spectroscopy techniques capable of detecting single molecules [3], waveguides [4], biosensors [5,6], and subwavelength optical applications such as nanoscale lithography [7].

SPPs have been widely studied in layered media [8–10]. However, modeling of layered devices is restricted to large scale numerical simulations [11,12]. These studies consider each layer as homogeneous or periodically modulated and calculate the reflection spectrum of the device using transmission or scattering matrices [13–16]. This method can be applied to nonhomogenous materials by approximating them as a large number of homogeneous layers.

Despite its frequent use, the scattering matrix method of modeling layered media is computationally expensive for highly nonhomogeneous media and does not easily allow the dominant optical interactions to be isolated. One example of a device for which this is the case is the hybrid photorefractive–plasmonic liquid crystal (LC) cell [17,18]. This device provides the means to manipulate and enhance SPP propagation. It consists of a thin gold layer, roughly 40 nm thick, adjacent to a LC cell. An SPP can be excited at the LC–Au interface via a high refractive index prism on the other side of the Au layer [19]. The SPP can then be manipulated by application of an electric field that reorients the LC near to the surface. Coupling between SPP is achieved by applying a periodically modulated voltage to the LC that produces a refractive index grating [20].

The response of a SPP at the interface between a gold layer and a LC is well understood [21]. However, due to the complexity of the device and the waveguide properties of the LC cell, the number of possible mode couplings in the device is relatively high. This makes it nearly impossible to isolate the dominant mechanisms and control parameters for SPP–SPP coupling using scattering matrix techniques.

In this paper we develop an approximation method that can be used to study the transfer of energy into and between different SPP modes. We consider the device as a set of different waveguides. Each waveguide is simple enough that analytic expressions for their modes can be obtained [22]. The interaction between the modes can then be considered as a perturbation. This method, which is similar to the tight binding approximation used in atomic physics [23], allows us to isolate the dominant interactions in the device and, hence, provides the means to increase efficiency without the need for a large scan of the parameter space. The model captures the salient features of the reflection spectrum without the need, for example, to consider the LC inhomogeneity and anisotropy.

We use the derived model to study the transfer of energy between SPP and guided modes in an example system that is comparable to a hybrid photorefractive–plasmonic LC cell. We calculate the response of the system to several control parameters including the gold thickness, grating wavenumber, and the grating strength. We also consider the role of the guided modes in the response of the system and how their effects can be manipulated to increase efficiency.

The model derived here is of wide general use and can be applied to understand the mode-mode interactions or to calculate the reflection spectrum of any layered system in which the modes can be easily approximated. Such devices include

metallic grating couplers [24] and planar–waveguide Bragg sensors [6]. The theory can also be applied to the study of nonlinear surfaces waves excited at the interface between a metal layer and a photorefractive crystal [25].

As the model derived here is an approximate model, it offers a significant reduction in computation time. Typical simulation times for this model are reduced by a factor of 100 when compared to a scattering matrix code. However, the key advantage to the method described in this paper is that, as a semi-analytic method, it offers significant insight into the underlying coupling mechanisms. Specifically, it allows the individual coupling coefficients that describe the interactions between the SPP and the guided modes to be isolated and quantified.

This paper is arranged as follows. In Section 2 we derive equations describing the interactions between the various optical fields and the refractive index grating. In Section 3 we analyze these equations to determine the key control parameters used to manipulate SPP in a layered device. Finally, our results are summarized in Section 4.

2. THEORY

In order to find the reflection spectrum of a photorefractive layered device, we make some simplifying assumptions. We assume that the device is planar and choose a coordinate system such that (see Fig. 1) the x direction is into the device, while the z direction is parallel to the input facet and in the direction of the SPP-coupling grating. The system is homogeneous in the y direction. The layers consist of a semi-infinite prism in the region $x < 0$ that represents the prism in a standard Kretschmann configuration [19]. Adjacent to the prism there is a gold layer that supports the SPPs followed by a range of dielectric layers, the last one of which is also semi-infinite. In this paper we consider the special cases of one and three dielectric layers corresponding to SPPs in the absence or presence of waveguide modes. We identify these layers as "cladding" and "core," as illustrated in Fig. 1.

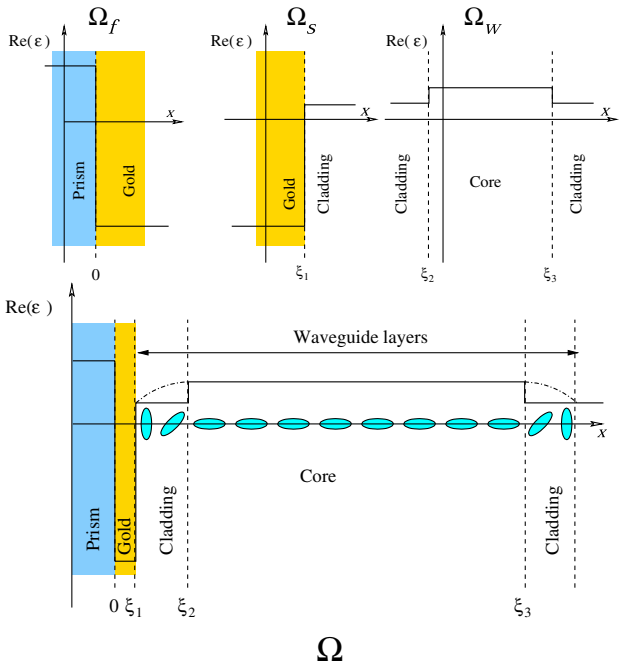

Fig. 1. Device schematic (bottom) showing its decoupled components (top) as specified in Eqs. (2). The ellipses represent the LC orientation in a photorefractive LC cell. They illustrate how the idealised dielectric layer geometry approximates the LC device.

Such a geometry can approximate not just a gold-coated isotropic dielectric waveguide, it is also applicable to hybrid photorefractive–plasmonic LC cells. In this case there are several additional assumptions made. This choice of geometry neglects the alignment layers and the LC anisotropy and inhomogeneity. As the alignment layers are thin, typically $\lesssim$100 nm, it is expected that neglecting them will not significantly impact the reflection spectrum of the device. The anisotropy and inhomogeneity of the LC is small relative to the isotropic part of the refractive index and, in principle, can be added as a perturbation. However, the effects of this perturbation are not expected to alter the reflection spectrum qualitatively.

A. Decoupled Waveguide

We consider time harmonic electric and magnetic fields and introduce the scaling $\tilde{\boldsymbol{\mathcal{E}}} = \boldsymbol{\mathcal{E}} e^{-i\omega t}/\sqrt{\epsilon_0}$, $\tilde{\boldsymbol{\mathcal{H}}} = \boldsymbol{\mathcal{H}} e^{-i\omega t}/\sqrt{\mu_0}$ for the electric and magnetic fields, respectively, and $\mathbf{r} = k_0\tilde{\mathbf{r}}$, where μ_0 and ϵ_0 are the permeability and permittivity of free space, respectively, $k_0 = 2\pi/\lambda$, and λ is the free space wavelength. Using this scaling Maxwell's equations can be written as

$$\begin{pmatrix} \mathcal{D} & -i \\ i\epsilon & \mathcal{D} \end{pmatrix} \begin{pmatrix} \boldsymbol{\mathcal{E}} \\ \boldsymbol{\mathcal{H}} \end{pmatrix} = 0, \tag{1}$$

where $\mathcal{D}$ is the curl operator such that $\mathcal{D}\boldsymbol{u} \equiv \nabla \times \boldsymbol{u}$ for a generic vector $\boldsymbol{u}$.

In general we must require that Eq. (1) is satisfied everywhere. However, in order to proceed analytically we first consider the waveguide geometry as physically separate from the SPP interface. We denote the waveguide geometry Ω_w, the plasmon interface Ω_s and the free space interface Ω_f. The composite geometry is their union, $\Omega = \Omega_w \cup \Omega_s \cup \Omega_f$ (see Fig. 1).

The dielectric functions in each medium can be written as

$$\epsilon_s = \begin{cases} \epsilon_r & x < \xi_1, \mathbf{r} \in \Omega_s \\ \epsilon_{\mathrm{cl}} & x > \xi_1, \mathbf{r} \in \Omega_s \end{cases}, \tag{2a}$$

$$\epsilon_w = \begin{cases} \epsilon_{\mathrm{cl}} & x < \xi_2, \mathbf{r} \in \Omega_w \\ \epsilon_{\mathrm{co}} & \xi_2 < x < \xi_3, \mathbf{r} \in \Omega_w \\ \epsilon_{\mathrm{cl}} & \xi_3 < x, \mathbf{r} \in \Omega_w \end{cases}, \tag{2b}$$

$$\epsilon_f = \begin{cases} \epsilon_{\mathrm{gl}} & x < 0, \mathbf{r} \in \Omega_f \\ \epsilon_m & 0 < x, \mathbf{r} \in \Omega_f \end{cases}, \tag{2c}$$

where $\epsilon_m = \epsilon_r + i\epsilon_i$, ϵ_r and ϵ_i are the real and imaginary parts of the gold dielectric constant, ϵ_{cl} is the dielectric constant in the cladding, ϵ_{co} the dielectric constant in the core, and ϵ_{gl} is the dielectric constant in the glass. We also define $L_{\mathrm{au}} = \xi_1$, $L_{\mathrm{cl}} = \xi_2 - \xi_1$, and $L_{\mathrm{co}} = \xi_3 - \xi_2$ for the thickness of the gold, cladding and core respectively. We consider optical and SPP modes that are bound in the x direction. Hence, we write a general expression for modes that can propagate in any direction in the y, z plane. We denote this propagation direction with the unit vector $\hat{\boldsymbol{\upsilon}}$, which is restricted to the y, z plane. We also define a vector $\hat{\boldsymbol{\upsilon}}_\perp$, a unit vector that is also restricted to

the y, z plane and is orthogonal to $\hat{\boldsymbol{\upsilon}}$. Using this notation the transverse magnetic solution to Maxwell's equations local to the plasmon interface is

$$\mathcal{H}_s = A_s \boldsymbol{H}_s(x) e^{in_s \hat{\boldsymbol{\upsilon}} \cdot \boldsymbol{r}}, \qquad \boldsymbol{r} \in \Omega_s, \tag{3}$$

where

$$\boldsymbol{H}_s(\boldsymbol{r}) = \begin{cases} \hat{\boldsymbol{\upsilon}}_\perp e^{\beta_{s1}(x-\xi_1)} & x < \xi_1 \\ \hat{\boldsymbol{\upsilon}}_\perp e^{-\beta_{s2}(x-\xi_1)} & x > \xi_1 \end{cases}, \tag{4}$$

with corresponding electric field $\boldsymbol{E}_s$ calculated using Eq. (1). Here, A_s is the mode amplitude, and the SPP effective index and decay constants are given by [1]

$$n_s = \sqrt{\frac{\epsilon_r \epsilon_{\mathrm{cl}}}{\epsilon_r + \epsilon_{\mathrm{cl}}}}, \qquad \beta_{s1} = \sqrt{\frac{-\epsilon_r^2}{\epsilon_r + \epsilon_{\mathrm{cl}}}}, \qquad \beta_{s2} = \sqrt{\frac{-\epsilon_{\mathrm{cl}}^2}{\epsilon_r + \epsilon_{\mathrm{cl}}}}. \tag{5}$$

The solutions in the waveguide are

$$\mathcal{H}_w = \sum_{q=0}^{N} A_q \boldsymbol{H}_q(x) e^{in_q \hat{\boldsymbol{\upsilon}} \cdot \boldsymbol{r}}, \qquad \boldsymbol{r} \in \Omega_w, \tag{6}$$

where n_q are the effective indices of the guided modes calculated using the Cauchy integral method [26–28] and A_q are the mode amplitudes. The fundamental mode is even and corresponds to $q = 0$. The modes with even indices have a magnetic field of

$$\boldsymbol{H}_q = \begin{cases} \hat{\boldsymbol{\upsilon}}_\perp \cos\left[\frac{L_{\mathrm{co}}\gamma_q}{2}\right] e^{(x-\xi_2)\beta_q}, & x < \xi_2, \\ \hat{\boldsymbol{\upsilon}}_\perp \cos\left[\left(x - \frac{\xi_3+\xi_2}{2}\right)\gamma_q\right], & \xi_2 < x < \xi_3, \\ \hat{\boldsymbol{\upsilon}}_\perp \cos\left[\frac{L_{\mathrm{co}}\gamma_q}{2}\right] e^{-(x-\xi_4)\beta_q}, & \xi_3 < x, \end{cases} \tag{7}$$

where $\gamma_q = \sqrt{\epsilon_{\mathrm{co}} - n_q^2}$ and $\beta_q = \sqrt{n_q^2 - \epsilon_{\mathrm{cl}}}$ [22]. The modes with odd indices have a magnetic field of

$$\boldsymbol{H}_q = \begin{cases} -\hat{\boldsymbol{\upsilon}}_\perp \sin\left[\frac{L_{\mathrm{co}}\gamma_q}{2}\right] e^{(x-\xi_2)\beta_q}, & x < \xi_2, \\ \hat{\boldsymbol{\upsilon}}_\perp \sin\left[\left(x - \frac{\xi_3+\xi_2}{2}\right)\gamma_q\right], & \xi_2 < x < \xi_3, \\ \hat{\boldsymbol{\upsilon}}_\perp \sin\left[\frac{L_{\mathrm{co}}\gamma_q}{2}\right] e^{-(x-\xi_3)\beta_q}, & \xi_3 < x. \end{cases} \tag{8}$$

The guided modes have corresponding electric field profiles, $\boldsymbol{E}_q$, calculated using Eq. (1). The solution at the interface is

$$\mathcal{H}_f = \boldsymbol{H}_f e^{in_f z}, \tag{9}$$

where

$$\boldsymbol{H}_f = \begin{cases} \hat{\boldsymbol{\upsilon}}_\perp e^{i\gamma_f x} + A_r \hat{\boldsymbol{\upsilon}}_\perp e^{-i\gamma_f x} & x < 0, \ \boldsymbol{r} \in \Omega_f, \\ A_t \hat{\boldsymbol{\upsilon}}_\perp e^{-\beta_f x} & x > 0, \ \boldsymbol{r} \in \Omega_f, \end{cases} \tag{10}$$

$\gamma_f = \sqrt{\epsilon_{\mathrm{gl}} - n_f^2}$, $\beta_f = \sqrt{n_f^2 - \epsilon_m}$, and A_r and A_t are the amplitudes of the reflected and transmitted fields. The free space modes have corresponding electric field $\boldsymbol{E}_f$, calculated using Eq. (1).

The waveguide modes are the standard odd and even planar waveguide modes [22] that satisfy the orthogonality condition

$$\int_{-\infty}^{+\infty} \boldsymbol{H}_p^* \cdot \boldsymbol{H}_q \mathrm{d}x \propto \delta_{pq}. \tag{11}$$

In order for our approximation to be valid, and that the device may be decomposed into three separate regions, we also require

$$\int_{-\infty}^{+\infty} \boldsymbol{H}_\alpha^* \cdot \boldsymbol{H}_\beta \mathrm{d}x \sim O(\eta), \tag{12}$$

where $\eta \ll 1$, $\alpha = \{s, f\}$ for the SPP and free space fields, respectively, $\beta = \{s, q\}$ for the SPP and guided modes, respectively, and $\alpha \neq \beta$.

B. Coupled Waveguide

The undetermined amplitudes in Eqs. (3), (6) and (10) are found by requiring that Maxwell's boundary conditions for the tangential components of the electric and magnetic fields are satisfied in terms of all the fields at $x = 0$. In order to achieve this we need to consider the composite waveguide structure and, hence, the interaction of all the modes.

As $\Omega_f \cap \Omega_w \neq 0$, $\Omega_f \cap \Omega_s \neq 0$ and $\Omega_s \cap \Omega_w \neq 0$ the solutions [Eqs. (3), (6), and (9)] will only be approximate solutions to Eq. (1) for $\boldsymbol{r} \in \Omega$. We consider the intersection of the different geometries as a perturbation that has the effect of coupling the different fields. We also consider the effect of a weak refractive index grating in the optical waveguide. The grating vector is parallel to the surface of the waveguide. Therefore, the effect of the grating is to diffract energy from the initial excitations into a series of higher diffracted orders traveling in different directions along the surface (see Fig. 2).

We write $\epsilon = \epsilon_1 + \eta(\bar{\epsilon}_g e^{i\boldsymbol{k}_g \cdot \boldsymbol{r}} + \bar{\epsilon}_g^* e^{-i\boldsymbol{k}_g \cdot \boldsymbol{r}}), \boldsymbol{r} \in \Omega$, where the superscript $*$ denotes the complex conjugate, $\epsilon_1 = \epsilon_s + \bar{\epsilon}_s = \epsilon_w + \bar{\epsilon}_w = \epsilon_f + \bar{\epsilon}_f$, $\boldsymbol{k}_g = \lambda/\Lambda[\hat{\boldsymbol{e}}_y \cos(\theta_g) + \hat{\boldsymbol{e}}_z \sin(\theta_g)]$, Λ is the grating spacing and θ_g is the propagation angle of the incoming field in the y, z plane with respect to the y axis. The dielectric perturbations are

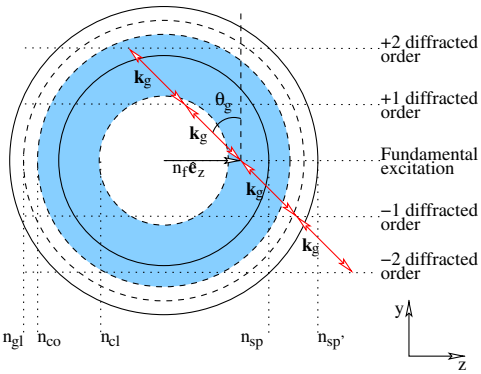

Fig. 2. Phase matching diagram showing the possible couplings between an incident field, with tangential wave vector $n_f \hat{\boldsymbol{e}}_z$, and all possible guided and plasmonic modes. The grating vector $\boldsymbol{k}_g$ is shown in red and makes and angle θ_g with the y axis. The region in which the guided modes exist is shaded in blue.

$$\bar{\epsilon}_s = \begin{cases} \epsilon_{\mathrm{gl}} - \epsilon_r & x < 0 \\ i\epsilon_i & 0 < x < \xi_1 \\ \epsilon_{\mathrm{co}} & \xi_2 < x < \xi_3 \\ 0 & \text{otherwise} \end{cases}, \tag{13a}$$

$$\bar{\epsilon}_w = \begin{cases} \epsilon_{\mathrm{gl}} - \epsilon_{\mathrm{cl}} & x < 0 \\ \epsilon_m - \epsilon_{\mathrm{cl}} & 0 < x < \xi_1 \\ 0 & \text{otherwise} \end{cases}, \tag{13b}$$

$$\bar{\epsilon}_f = \begin{cases} \epsilon_{\mathrm{cl}} - \epsilon_m & \xi_1 < x < \xi_2 \\ \epsilon_{\mathrm{co}} - \epsilon_m & \xi_2 < x < \xi_3 \\ \epsilon_{\mathrm{cl}} - \epsilon_m & \xi_3 < x \\ 0 & \text{otherwise} \end{cases}. \tag{13c}$$

The grating may exist in both the core and cladding layers and potentially have a different phase in each layer, as is the case for photorefractive LC cells [29]. Therefore, we consider the grating as having a component in the cladding layer nearest the gold and a component in the core,

$$\bar{\epsilon}_g = \begin{cases} \bar{\epsilon}_{g,\mathrm{cl}} & \xi_1 < x < \xi_2 \\ \bar{\epsilon}_{g,\mathrm{co}} & \xi_2 < x < \xi_3 \end{cases}. \tag{14}$$

We note that a more complete description of the hybrid LC photorefractive system could be made by incorporating the LC anisotropy and inhomogeneity as part of the perturbation. However, we do not do so, as the aim of this paper is to consider the dominant effects present in the system while keeping the model simple enough to gain a thorough understanding of the system.

We now return to the boundary condition at $x = 0$. In general, $n_f \neq n_s \neq n_q$ and we cannot meet the boundary conditions for all n_f. If this were the case, then it would be impossible to couple into the guided and plasmonic modes except for the special cases $n_f = n_s$ or $n_f = n_q$.

To overcome this problem we assume that the surface plasmon and the guided modes all have a spatial dependence of the form $e^{i\boldsymbol{k}_f^{(m)}\cdot\boldsymbol{r}}$, where m denotes the diffracted order, $\boldsymbol{k}_f^{(m)} = n_f\hat{\boldsymbol{e}}_z + m\boldsymbol{k}_g$, and $\hat{\boldsymbol{e}}_z$ is a unit vector in the z direction. The result of this assumption is that we cannot satisfy Maxwell's equations. However, if we assume that the error induced by this assumption is small, it is possible to make progress. Physically, this condition tells us that energy can couple into the guided and plasmonic modes if the respective effective indices are close enough to n_f.

We consider the expansion $\boldsymbol{\mathcal{E}} = \boldsymbol{\mathcal{E}}_0 + \eta\boldsymbol{\mathcal{E}}_1 + O(\eta^2)$ and $\boldsymbol{\mathcal{H}} = \boldsymbol{\mathcal{H}}_0 + \eta\boldsymbol{\mathcal{H}}_1 + O(\eta^2)$, where $\boldsymbol{\mathcal{E}}_0$ and $\boldsymbol{\mathcal{H}}_0$ are the leading order solutions to Maxwell's equations that are determined up to a constant amplitude [see Eqs. (3), (6), and (9)]. We now consider all diffracted orders of the incident field, the SPP and the guided modes. Extending the solutions defined in Eqs. (4), (7), (8), and (10), such that the propagation vector is defined by $\boldsymbol{k}_f^{(m)}$, we substitute

$$\boldsymbol{\mathcal{H}}_s^{(m)} = A_s^{(m)}\boldsymbol{H}_s^{(m)}(x)e^{i\boldsymbol{k}_f^{(m)}\cdot\boldsymbol{r}}, \tag{15}$$

$$\boldsymbol{\mathcal{H}}_w^{(m)} = \sum_{q=1}^{N} A_q^{(m)}\boldsymbol{H}_q^{(m)}(x)e^{i\boldsymbol{k}_f^{(m)}\cdot\boldsymbol{r}}. \tag{16}$$

into Eq. (1) and retain terms $O(\eta)$, which oscillate with spatial dependence $e^{i\boldsymbol{k}_f^{(m)}\cdot\boldsymbol{r}}$. The result is a set of nonhomogeneous equations for the first order correction to the electric and magnetic fields. By eliminating terms that exhibit linear growth [21,30] we obtain an equation for the SPP coupling,

$$\begin{aligned}(\kappa_{s,s} + P_s\overline{\delta n}_s^{(m)})A_s^{(m)} + \kappa_{s,f}A_t^{(m)} + \sum_{q=0}^{N}\kappa_{s,q}A_q^{(m)} + \chi_{s,s}A_s^{(m+1)} \\ + \chi_{s,f}A_t^{(m+1)} + \sum_{q=0}^{N}\chi_{s,q}A_q^{(m+1)} + \chi_{s,s}^*A_s^{(m-1)} + \chi_{s,f}^*A_t^{(m-1)} \\ + \sum_{q=0}^{N}\chi_{s,q}^*A_q^{(m-1)} = 0,\end{aligned} \tag{17a}$$

and a set of equations for the coupling into the guided modes,

$$\begin{aligned}P_p\overline{\delta n}_p^{(m)}A_p^{(m)} + \kappa_{p,f}A_t^{(m)} + \kappa_{p,s}A_s^{(m)} + \sum_{q=0}^{N}\kappa_{p,q}A_q^{(m)} + \chi_{p,s}A_s^{(m+1)} \\ + \chi_{p,f}A_t^{(m+1)} + \sum_{q=0}^{N}\chi_{p,q}A_q^{(m+1)} + \chi_{p,s}^*A_s^{(m-1)} + \chi_{p,f}^*A_t^{(m-1)} \\ + \sum_{q=0}^{N}\chi_{p,q}^*A_q^{(m-1)} = 0.\end{aligned} \tag{17b}$$

where $\overline{\delta n}_s^{(m)} = |\boldsymbol{k}_f^{(m)}| - n_s$ and $\overline{\delta n}_p^{(m)} = |\boldsymbol{k}_f^{(m)}| - n_p$, $|\boldsymbol{k}_f^{(m)}| = [(m\lambda/\Lambda)^2 + (2n_f m\lambda/\Lambda)\sin(\theta_g) + n_f^2]^{1/2}$. The SPP power is

$$P_s = \frac{n_s(\beta_{s1}\epsilon_{\mathrm{cl}} + \beta_{s2}\epsilon_r)}{\beta_{s1}\epsilon_{\mathrm{cl}}\beta_{s2}\epsilon_r}, \tag{18}$$

and P_p is the power of the pth guided mode. For sufficiently large waveguide cores, typically $L_{\mathrm{co}} \gg \epsilon_{\mathrm{cl}}/\gamma_p$ and $L_{\mathrm{cl}} \gg \epsilon_{\mathrm{co}}/\gamma_p$, this can be written as

$$P_p \approx \frac{n_p L_{\mathrm{co}}}{\epsilon_{\mathrm{co}}}. \tag{19}$$

The coupling coefficients are given by the overlap of the fields with the dielectric perturbation,

$$\kappa_{\alpha,\beta} = \int_{-\infty}^{\infty}\bar{\epsilon}_\alpha\boldsymbol{E}_\alpha^{(m)}\cdot\boldsymbol{E}_\beta^{(m)}\mathrm{d}x, \tag{20}$$

$$\chi_{\alpha,\beta} = \int_{-\infty}^{\infty}\bar{\epsilon}_g\boldsymbol{E}_\alpha^{(m)}\cdot\boldsymbol{E}_\beta^{(m+1)}\mathrm{d}x, \tag{21}$$

where $\alpha,\beta = \{s,q,f\}$ for the SPP, m-th guided mode and free space field, respectively. Of specific interest is the coupling coefficients relating to the SPP–SPP interaction via the refractive index grating

$$\begin{aligned}\chi_{s,s} = \epsilon_{g,\mathrm{cl}}\frac{(n_s^2 + \beta_{s2}^2)(1 - e^{-2\beta_{s2}L_{\mathrm{cl}}})}{2\beta_{s2}\epsilon_{\mathrm{cl}}^2} \\ - \epsilon_{g,\mathrm{co}}\frac{(n_s^2 + \beta_{s2}^2)(1 - e^{-2\beta_{s2}L_{\mathrm{co}}})e^{-2\beta_{s2}L_{\mathrm{cl}}}}{2\beta_{s2}\epsilon_{\mathrm{cl}}^2},\end{aligned} \tag{22}$$

which we will refer to in the analysis of the mode interactions. We now return to the source terms that drive these

interactions. To determine the amplitude of the reflected field we require that Maxwell's boundary conditions are satisfied at the glass–gold boundary, $x = 0$. Specifically, we write the boundary conditions on the magnetic and electric fields as

$$\langle \boldsymbol{H} \rangle_s^{(m)} A_s^{(m)} + A_t^{(m)} + \sum_{q=1}^{N} \langle \boldsymbol{H} \rangle_q^{(m)} = \delta_{0m} + A_r^{(m)}, \tag{23}$$

and

$$\langle \boldsymbol{E} \rangle_s^{(m)} A_s^{(m)} - \frac{\beta_f^{(m)}}{\epsilon_2} A_t^{(m)} + \sum_{q=1}^{N} \langle \boldsymbol{E} \rangle_q^{(m)} = \frac{i\gamma_f^{(m)}}{\epsilon_1} (\delta_{0m} - A_t^{(m)}), \tag{24}$$

where $\langle \cdot \rangle$ denotes the projection of the corresponding field at $x = 0$ onto the interface. Equation (17), (23), and (24) are a system of $(M + 3)(2N + 1)$ linear equations, where M is the number of guided modes and N is the number of diffracted orders considered.

C. No Guided Modes

The first case we consider is that of a single cladding layer device. This corresponds to a photorefractive LC cell that is aligned homeotropically on each surface. The result of this alignment is that there is no waveguide region for the guided modes and any grating induced in the LC will extend into the bulk.

If this is the case then, in the absence of the grating, we have a standard Kretschmann configuration [19]. In this case the geometry is simple enough that the reflection spectrum can be derived exactly. This allows us to verify that our model predicts the correct spectrum qualitatively. Here, Eqs. (17), (23), and (24) reduce to a system of three equations for the unknown amplitudes A_s, A_t, and A_r,

$$\begin{pmatrix} -1 & 1 & 1 \\ 1 & -i\tilde{\beta}_f & i\tilde{\beta}_{s1} \\ 0 & \kappa_{s,f} & i\tilde{\kappa}_{s,s} + \widetilde{\delta n}_s \end{pmatrix} \begin{pmatrix} A_r \\ A_t \\ \tilde{A}_s \end{pmatrix} = \begin{pmatrix} 1 \\ 1 \\ 0 \end{pmatrix}, \tag{25}$$

where $\tilde{A}_s = e^{-\beta_{s1} L_{au}} A_s$, $\widetilde{\delta n}_s = P_s \overline{\delta n}_s e^{\beta_{s1} L_{au}}$, $\tilde{\kappa}_{s,s} = -i\kappa_{s,s} e^{\beta_{s1} L_{au}}$, $\tilde{\beta}_f = -(\beta_f \epsilon_{gl}/\gamma_f(\epsilon_m))$, and $\tilde{\beta}_{s1} = -(\beta_{s1}\epsilon_{cl}/\gamma_f(\epsilon_m))$. Solving Eq. (25) we obtain the reflected amplitude,

$$A_r = \frac{(1 + i\tilde{\beta}_f)(i\tilde{\kappa}_{s,s} + \widetilde{\delta n}_s) - (1 - i\tilde{\beta}_{s1})\kappa_{s,f}}{(1 - i\tilde{\beta}_f)(i\tilde{\kappa}_{s,s} + \widetilde{\delta n}_s) - (1 + i\tilde{\beta}_{s1})\kappa_{s,f}}. \tag{26}$$

The reflected intensity is given by $I_r = |A_r|^2$, which has a minimum at

$$n_f \approx n_s + \frac{\kappa_{s,f} e^{-\beta_{s1} L_{au}}}{P_s} \left(\frac{\beta_{s1}^2 \epsilon_{gl}^2 + n_s^2 \epsilon_m^2 - \epsilon_{gl} \epsilon_m^2}{\beta_{s1}^2 \epsilon_{gl}^2 - n_s^2 \epsilon_m^2 + \epsilon_{gl} \epsilon_m^2} \right). \tag{27}$$

The addition of a grating to this geometry causes the fields to be coupled through the coupling coefficients, χ. There are two possible coupling mechanisms that are distinct under the approximations used. The first is the coupling between the incoming field and the diffracted SPP, $\chi_{s,f}$. The second is the coupling between the different SPP orders, $\chi_{s,s}$. Due to the presence of the gold layer, the free space field is relatively weak in the core and cladding layers. Therefore, $\chi_{s,s} \gg \chi_{s,f}$ and we can neglect $\chi_{s,f}$. This suggests that coupling is only strong if the grating vectors are sufficient to match from one SPP to another.

One of the key aims of this work is to obtain an estimate of the coupling strength. We achieve this by considering a system where the grating vector is sufficiently long that energy is coupled only between three families of modes: the fundamental family of modes and the plus and minus one diffracted orders. This case is analogous to the case where the grating vector is short such that more modes can be present but the coupling is also weak and very little energy is diffracted beyond the first modes.

Using the fact that there are no guided modes, and there are only three families of modes (in this case a family of modes consists of a SPP and the free space field), we can invert the linear system analytically. The linear system we must solve, written in block matrix form, is

$$\begin{pmatrix} K_{+1} & \chi_{+1,0} & 0 \\ \chi_{0,+1} & K_0 & \chi_{-1,0} \\ 0 & \chi_{0,-1} & K_{-1} \end{pmatrix} \begin{pmatrix} \boldsymbol{A}_{+1} \\ \boldsymbol{A}_0 \\ \boldsymbol{A}_{-1} \end{pmatrix} = \begin{pmatrix} \boldsymbol{0} \\ \boldsymbol{S} \\ \boldsymbol{0} \end{pmatrix}, \tag{28}$$

where $K_0 \boldsymbol{A}_0 = \boldsymbol{S}$ is the linear system we solved in the case where no grating is present. The additional terms describe the coupling into and out of the various diffracted orders. Solving Eq. (28) we obtain

$$\boldsymbol{A}_0 = P^{-1} \boldsymbol{S}, \tag{29a}$$

and

$$\boldsymbol{A}_{\pm 1} = -K_{\pm 1}^{-1} \chi_{0,\pm 1} P^{-1} \boldsymbol{S}, \tag{29b}$$

where $P = K_0 - \chi_{0,+1} K_{+1}^{-1} \chi_{+1,0} - \chi_{0,-1} K_{-1}^{-1} \chi_{-1,0}$. As we are able to neglect the coupling induced by the free space field $\chi_{s,f}$, we find that all elements of the matrices $\chi_{0,+1} K_{+1}^{-1} \chi_{+1,0}$ and $\chi_{0,-1} K_{-1}^{-1} \chi_{-1,0}$ are zero except for the bottom right entry. Hence, the reflected field is

$$A_r^{(0)} = \xi_0 [(1 + i\tilde{\beta}_f^{(0)})X - (1 - i\tilde{\beta}_{s1}^{(0)})\kappa_{s,f}^{(0)}], \tag{30}$$

and the diffracted fields are

$$A_r^{(\pm 1)} = \frac{2i\zeta_0 \tilde{\chi}_{s,s}^{(0,\pm 1)} \kappa_{s,f}^{(0)} (\tilde{\beta}_f^{(\pm 1)} + \tilde{\beta}_{s1}^{(\pm 1)})}{(i\tilde{\kappa}_{s,s} + \widetilde{\delta n}_s^{(\pm 1)})(i\tilde{\beta}_f^{(\pm 1)} - 1) + \kappa_{s,f}^{(\pm 1)} (i\tilde{\beta}_{s1}^{(\pm 1)} + 1)}, \tag{31}$$

where $\tilde{\chi}_{s,s} = \chi_{s,s} e^{\tilde{\beta}_{s1} L_{au}}$,

$$\zeta_0 = \frac{1}{(1 - i\tilde{\beta}_f^{(0)})X - (1 + i\tilde{\beta}_{s1}^{(0)})\kappa_{s,f}^{(0)}}, \tag{32}$$

$$X = i\tilde{\kappa}_{s,s} + \widetilde{\delta n}_s^{(0)} - \zeta^{(+1)} - \zeta^{(-1)}, \tag{33}$$

$$\zeta^{(\pm 1)} = \frac{(i\tilde{\beta}_f^{(\pm 1)} - 1)\tilde{\chi}_{s,s}^{(0,\pm 1)} \tilde{\chi}_{s,s}^{(\pm 1,0)}}{\kappa_{s,f}^{(\pm 1)} (1 + i\tilde{\beta}_{s1}^{\pm 1}) - (\widetilde{\delta n}_s^{(\pm 1)} + i\tilde{\kappa}_{s,s})(1 + i\tilde{\beta}_f^{\pm 1})}, \tag{34}$$

and the superscripts denote the diffracted order. Equation (31) describes the diffracted energy into the plus or minus one

diffracted orders and has been verified through comparison to the solution of the full system.

Equations (30) and (31) are valid in the absence of guided modes, while the more complex Eqs. (17), (23), and (24) include the contribution to SPP–SPP coupling by the waveguide modes. These equations will be analyzed in detail to provide further insight into the coupling mechanisms in the next section.

3. ANALYSIS

A. Introduction

In the previous section we have derived a set of equations that describe the effect of the refractive index grating on SPP–SPP coupling.

These equations are a powerful, if nontrivial, tool to analyze the effect of the various system parameters on SPP–SPP coupling. In this section we apply the coupling equations in the absence of guided modes, Eqs. (30) and (31), to study the effect on SPP–SPP coupling of three key parameters that can be readily changed in experiments, namely the thickness of the gold (Section 3.B), the grating wave number (Section 3.C) and the coupling strength (Section 3.D). We include the effect of the guided modes using Eqs. (17), (23), and (24) in Section 3.E.

The approximation Eq. (31) used in Sections 3.B–3.D is derived in the limit of semi-infinite decoupled systems with only the fundamental and the ±1 diffracted orders. Here, we use it to study finite, weakly coupled systems with potentially many diffracted orders. Hence, we cannot expect the approximation to give very accurate results. However, we show in this section that not only does it capture the qualitative features of these systems, but its predictions are in rough quantitative agreement with full numerical simulations. In each case we have checked that the difference between the asymptotic and the "exact" results obtained using an *S*-matrix code is not significantly large. A typical comparison of the two outputs is shown in Fig. 4. The parameter values used in all simulations are listed in Table 1.

B. Effect of Gold Thickness

The gold thickness has a two-sided effect on SPP–SPP coupling. On the one hand, the maximum amplitude of the SPP decays to zero for large gold thickness, because in this limit the incident field has decayed to zero before it can couple to the SPP. On the other hand, for very thin gold layers the SPP becomes wider and less intense. In the limit of a vanishing small gold layer the exciting field suffers very little absorption, but the SPP is so delocalized that its maximum amplitude becomes negligible. This phenomenon is illustrated in Fig. 3, where we have plotted the minimum of the reflected field as a function of the gold thickness (solid line). This line was obtained using Eq. (30) and shows that there is a clear optimum thickness (approximately 38 nm) for coupling the external field to the SPP.

The energy diffracted by the grating in the first diffracted orders, computed using Eq. (31), follows the same trend of the fundamental SPP (dashed and dash–dotted lines in Fig. 3). This observation is to be expected on physical grounds (the coupling happens to the right of the gold layer and its physical mechanism is independent of the gold thickness). It is also expected on mathematical grounds because the SPP–SPP coupling coefficient, Eq. (22), does not depend on the gold thickness. The difference in intensity between the ±1 diffracted orders is due to the fact that the grating angle θ_g is equal to θ_m, the grating angle that matches perfectly the fundamental and the +1 SPP,

$$\theta_m = \arcsin\left(\frac{|k_g|}{2n_s}\right). \tag{35}$$

Table 1. Default Parameter Values Used in All Figures[a,b]

$\Lambda = 4\times10^{-6}$ m	$L_{au} = 40\times10^{-9}$ m	$\epsilon_{g,cl} = \epsilon_{g,co} = 0.02$
$\epsilon_{gl} = 3.36$	$\epsilon_{cl} = 2.50$	$\epsilon_{co} = 2.76$
$\theta_g = \theta_m$	$\lambda = 850\times10^{-9}$ m	$\epsilon_r = -31.14$
$\epsilon_i = 2.19$		

[a]Λ is the grating wavelength; L_{au} is the gold layer thickness; $\epsilon_{g,[cl,co]}$ is the amplitude of the dielectric grating in the cladding and core layer, respectively; $\epsilon_{gl,cl,co}$ is the dielectric permeability of the glass prism, cladding and core, respectively; ϵ_r and ϵ_i are the real and imaginary parts of the dielectric permeability of the gold; θ_g is the angle that the grating makes with the *y*-axis; θ_m is the grating angle that perfectly matches the fundamental and the +1 diffracted SPP for a given Λ; and λ is the light wavelength.

[b]The dielectric permeability of the gold is taken from [31].

C. Effect of the Grating Wave Number

The key to understanding the effect of grating spacing is Fig. 2: for large values of the grating spacing (small grating wave numbers) the fundamental SPP is coupled equally between the ±1 modes. This is confirmed by Fig. 4, which plots the maximum of the relative intensity of the first diffracted orders as a function of the grating spacing. The predicted amplitudes of the ±1 modes converge to the same values for large grating spacings. Moreover, in this parameter region there is significant coupling to higher order modes; this is indicated by the growing difference between asymptotic and *S*-matrix results.

As the grating spacing decreases, the amplitude of the two first diffracted orders become very different. The +1 mode is, in the case of Fig. 4, perfectly matched and its amplitude grows, while the −1 is more and more mismatched and its amplitude decreases.

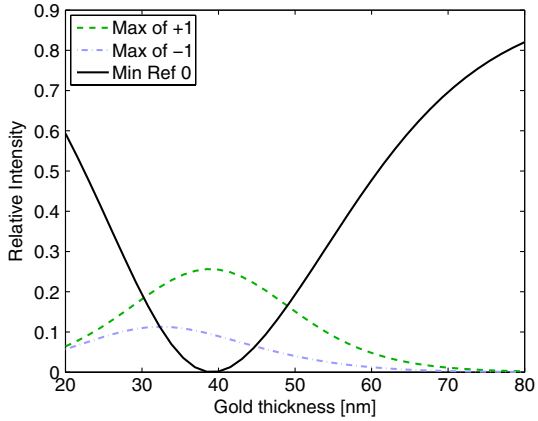

Fig. 3. Plot of the maximum of the relative intensity of the first diffracted orders and of the minimum of the reflected intensity as a function of the gold layer thickness. The curves are calculated using Eqs. (30) and (31) for the fundamental and first diffracted orders, respectively. The cladding is semi-infinite (no guided modes). All other parameters are as in Table 1.

The small peak/trough visible in the numerical curves of Fig. 4 at $\Lambda \simeq 1.1$ μm is caused by the coupling of the surface SPP localized at the interface between the gold and the cladding (right SPPs) to those at the interface between the prism and the gold layer (left SPPs). The effective refractive indices of the two SPPs are given by n_s in Eq. (5), using ϵ_{cl} and ϵ_{gl} for the left and right SPPs, respectively. A grating vector $\boldsymbol{k}_g$ at an angle $\theta_g = \theta_m$ from the vertical (see Fig. 2) can couple the fundamental right SPP with the first diffracted order of the left SPP if $|\boldsymbol{k}_g|$ satisfies

$$|\boldsymbol{k}_g|^2 = \frac{n_{s'}^2 - n_s^2}{2}, \tag{36}$$

where n_s and $n_{s'}$ are the effective refractive indices of the right and left SPPs, respectively. With the parameter values used in Fig. 4, this coupling occurs at $|\boldsymbol{k}_g| \simeq 0.73$, which correspond to a grating wavelength $\Lambda_g \simeq 1.17$ μm and is in agreement with the analytical estimate plotted in Fig. 4. The numerical estimate of the grating spacing in Fig. 4 is 1.09 μm. The difference between this value and that given by Eq. (36) may be attributed to the finite thickness of the gold: this has the effect of decreasing $n_{s'}^2 - n_s^2$ and, hence, $|\boldsymbol{k}_g|$. It is interesting to note that the analytical approximation captures the presence of this additional SPP, even though it is not explicitly included in the derivation of the model. On the other hand, while the numerical scattering code predicts a small dip in the intensity of the +1 mode, the analytical approximation predicts a small peak.

The results in Fig. 4 are directly comparable to our previously published experimental work on photorefractive–plasmonic LC cells, see Fig. 9 of [18]. The approximation described here captures the large grating pitch behavior of the experimental system. However, in the experimental system the diffraction efficiency is seen to drop off at grating pitches below 4 μm. This is attributed to the stiffness of the LC. As the LC physics are not included in the approximate model, we do not capture this behavior and do not see a drop off in relative intensity until a much smaller grating pitch.

D. Effect of the Coupling Strength

The energy transfer to diffracted orders is not a monotonically increasing function of the coupling strength, ϵ_g. As can be seen from Fig. 5, the intensity of the first diffracted orders at first increases with ϵ_g, but then decreases. The decrease is mild, according to the asymptotic model, and is due to the fact that ϵ_g appears linearly in the numerator of $A_r^{(\pm 1)}$ in Eq. (31), but appears quadratically in its denominator. The decrease is steeper, according to the *S*-matrix code, with an even sharper decline once ϵ_g is sufficiently large.

Figure 5 is comparable to our previously published experimental work (see Fig. 8a of [18]). Experimentally, the diffraction efficiency is seen to initially grow sharply with voltage until it reaches a peak at approximately 12 V; for a voltage greater than 12, the diffraction efficiency is seen to decrease slightly. While the voltage response of a LC is not strictly proportional to the grating strength, the approximate method developed here provides an explanation for this behavior, which was previously attributed to nonlinearities in the alignment layers [18].

The general behavior of the intensity of the ±1 diffracted orders can be understood by making reference to Fig. 6. In this figure we have chosen $\Lambda = 1$ μm to limit the number of diffracted orders and, thus, simplify the interaction. For weak coupling strength (top left panel of Fig. 6), energy is transferred from the fundamental SPP to the first diffracted order. As the coupling strength is increased, at first the only effect is to increase the amount of energy coupled out (top right panel of Fig. 6). However, if the coupling strength is increased even further, then energy starts to flow from the diffracted order back into the fundamental and also, depending on the configuration, to other diffracted orders. This effect is more pronounced at perfect resonance and the spectrum of the amplitude of the fundamental and diffracted order as a function of the reflection angle develops multiple peaks (bottom panels of Fig. 6).

E. Effect of the Guided Modes

The guided modes add another level of complexity to the problem. Here, we focus on their role on SPP–SPP coupling rather than on their effect on the spectral response of a gratingless device. We analyze their effect in the three cases

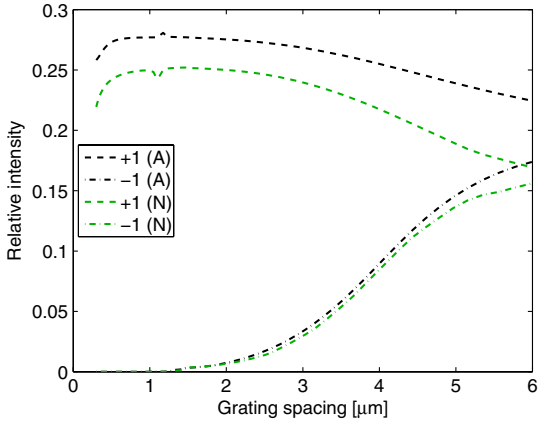

Fig. 4. Plot of the maximum of the intensity of the first diffracted orders scaled to that of the input beam as a function of the grating spacing Λ. The curves are computed numerically (N) or using the analytical model (A) given by Eq. (31). The cladding is semi-infinite (no guided modes). All other parameters are as in Table 1.

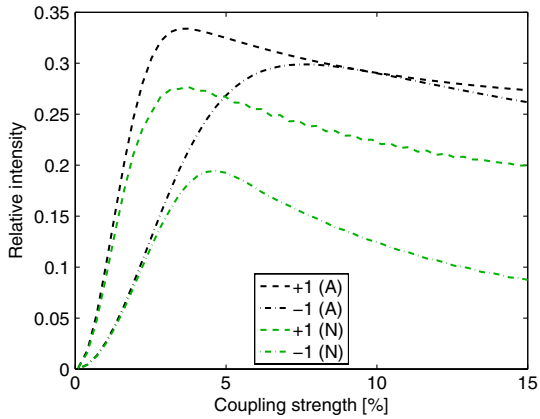

Fig. 5. Plot of the maximum of the intensity of the first diffracted orders, scaled to that of the input beam, as a function of the coupling strength $\epsilon_{g,\mathrm{cl}}$. The curves are computed numerically (N) or using the analytical model (A) given by Eq. (31). The cladding is semi-infinite (no guided modes). All other parameters are as in Table 1.

illustrated in Figs. 7–9. In all these figures the top panels display the reflection spectrum computed using the approximate model [Eqs. (30) and (31)], equivalent to the full model [Eqs. (17), (23), and (24)] with the coupling coefficients associated with the guided modes set to zero. The spectra in the middle and bottom panels take into account the guided modes and are computed using the full model [Eqs. (17), (23), and (24)] and a fully numerical scattering matrix algorithm [13–16], respectively.

If the grating is in the cladding (Fig. 7), the main coupling mechanism between different plasmonic diffracted orders is the direct grating-mediated SPP–SPP coupling in the cladding. The guided modes play no significant role and their main effect is to complicate the spectral response. A comparison between the top and the other two panels of Fig. 7 shows that the inclusion of the guided modes does not alter significantly the maximum of the first plasmonic diffracted order (approximately 27% in all panels). On the other hand, the guided modes introduce additional lines in the spectrum of the reflected field that correspond to their resonant frequencies.

A comparison between the middle and bottom panel of Fig. 7 reveals the strengths and limitations of the full model [Eqs. (17), (23), and (24)]. The model captures well the plasmon region and the dips in the intensity of the +1 diffracted order caused by the waveguide modes. In this region the model is both qualitatively and quantitatively accurate. However, the model becomes less accurate as we approach the region of total internal reflection (approximately 59° in the case represented in Fig. 7). The main difference between the two models is the waveguide mode line near 61° that is present in the *S*-matrix spectrum, but appears as a small dip at approximately 60.5° in the full model result. There is a mode of the waveguide that has index $n \simeq 1.6$, corresponding approximately to the dip in the numerical simulation. However, this mode has a low decay rate in the cladding and, hence, a very strong overlap with the gold and the prism.

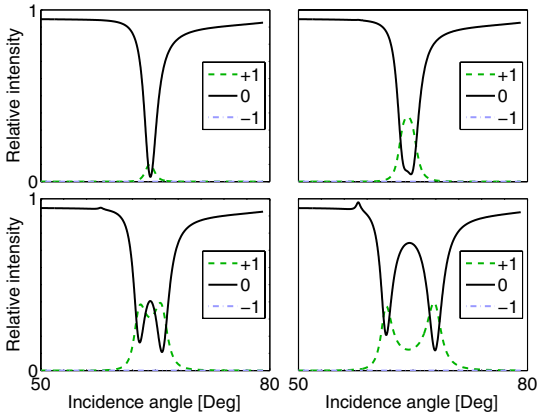

Fig. 6. Plot of the relative intensity of the reflected fundamental beam and diffracted orders as a function of the angle of incidence of the beam predicted by Eqs. (30) and (31), for $\epsilon_{g,\mathrm{cl}} = \{0.01, 0.03, 0.06, 0.12\}$ left to right, top to bottom, respectively, and $\Lambda = 1$ μm. The cladding is semi-infinite (no guided modes). All other parameters areas in Table 1.

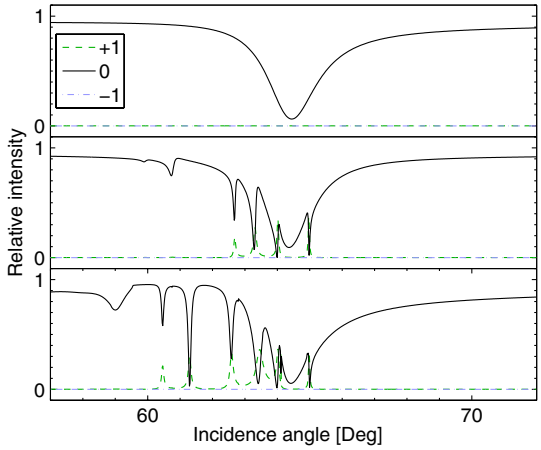

Fig. 8. Effect of guided modes for thick cladding, no grating in the cladding. Reflection spectrum computed using (top panel) Eqs. (30) and (31), i.e., no guided modes; (middle panel) Eqs. (17), (23), and (24); and (bottom panel) an *S*-matrix code. Left cladding thickness, $L_{\mathrm{cl}} = 600$ nm; core width, $L_{\mathrm{co}} = 2.5$ μm; semi-infinite right cladding, $\Lambda = 1$ μm, $\epsilon_{g,\mathrm{cl}} = 0$. All other parameters are as in Table 1.

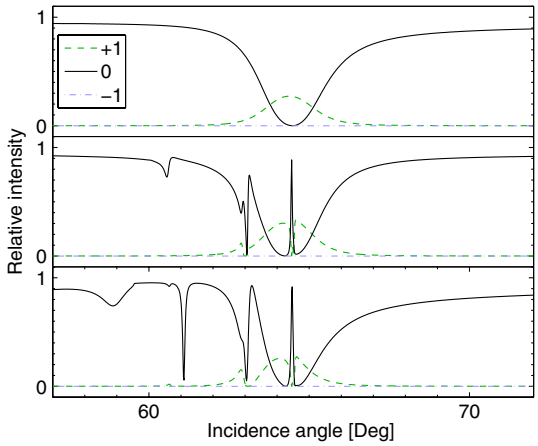

Fig. 7. Effect of guided modes for thick cladding, no grating in the core. Reflection spectrum computed using (top panel) Eqs. (30) and (31), i.e., no guided modes; (middle panel) Eqs. (17), (23), and (24); and (bottom panel) an *S*-matrix code. Left cladding thickness, $L_{\mathrm{cl}} = 600$ nm; core width, $L_{\mathrm{co}} = 2.5$ μm; semi-infinite right cladding, $\Lambda = 1$ μm, $\epsilon_{g,\mathrm{co}} = 0$. All other parameters are as in Table 1.

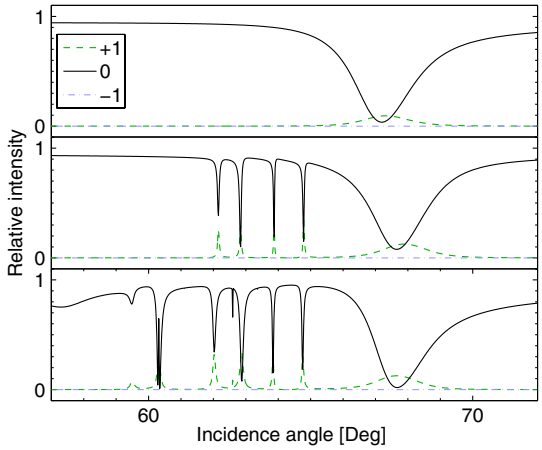

Fig. 9. Effect of guided modes for thin cladding, no grating in the cladding. Reflection spectrum is computed using (top panel) Eqs. (30) and (31), i.e., no guided modes; (middle panel) Eqs. (17), (23), and (24); and (bottom panel) an *S*-matrix code. Left cladding thickness, $L_{\mathrm{cl}} = 100$ nm; core width, $L_{\mathrm{co}} = 2.5$ μm; semi-infinite right cladding, $\Lambda = 1$ μm, $\epsilon_{g,\mathrm{cl}} = 0$. All other parameters are as in Table 1.

The correction due to this overlap is enough to push the mode a large distance from the original position.

The situation is rather different if the grating is in the core (Fig. 8). In this case the main coupling mechanism between different plasmonic orders is mediated through the guided modes. In the case of a thick cladding, there is no SPP–SPP coupling if modes are not considered (top panel of Fig. 8), while SPP–SPP coupling at the wavelengths of the guided modes can be observed if these are included (middle and bottom panels of Fig. 8).

Even if the guided modes are not immediately resonant with the SPP, their net effect is to enhance the SPP–SPP coupling. In Fig. 9 we analyze a thin cladding case. The cladding is sufficiently thin that the SPPs reach the core and are directly coupled by the grating there (top panel of Fig. 9). If we include the guided modes we observe two effects (middle and bottom panels of Fig. 9); there are additional resonances in the spectrum that correspond to the guided modes. More interestingly, the amplitude of the diffracted SPP is increased, from 9% to approximately 13%, even though no guided mode is directly resonant with the SPP. This indicates that the guided modes can be beneficial to the exchange of energy between SPPs and, possibly, SPP–SPP photorefractive gain.

4. SUMMARY

In this paper we have derived and analyzed an approximate set of equations that describe the response of a photorefractive layered device. These equations offer a significant reduction in computation time, approximatly a factor of 100 when compared to an S matrix code, and capture the salient features of any layered device with photorefractive and metalic layers and are a powerful analytical tool to dissect the optical interactions between SPPs, waveguide modes and incident fields, which are hard to estimate otherwise.

The equations are derived assuming an idealized geometry that also captures the features of the photorefractive LC cell. These equations can, in principle, be extended to consider the effects of the anisotropy and inhomogeneity of the LC as a perturbation. However, these effects are not expected to be significant in reproducing the main features of the reflection spectrum.

In this paper we have considered the cases of one and three dielectric layer devices adjacent to a standard two layer SPP interface. These geometries were chosen as they are simple enough that the modes of the individual waveguides can be found analytically. Considering the interaction between the waveguides and an external field allows the reflection spectrum to be obtained. Further, including the effect of a weak dielectric grating in the dielectric allows diffraction between different families of modes to be considered.

The derived model has been compared to numerical simulations and shows strong qualitative agreement. Further, a simplified model that neglects the modes in the LC waveguide has been derived to simplify the analysis and identify the salient features of the physics of these devices and of SPP–SPP photorefractive coupling.

Through careful analysis of the two models the effects of gold thickness, grating strength, grating vector, and the presence of guided modes have been studied. We have shown that an optimum gold thickness exists. This layer must be thick enough to support an SPP, yet thin enough that energy from the incident field can penetrate it to feed energy into the SPP. For the parameters studied here this thickness is approximately 38 nm.

The effect of the grating strength is somewhat surprising as simply increasing the modulation of the dielectric constant does not produce a monotonically increasing diffraction efficiency. Rather, there is an optimum grating strength above which energy couples back from the $+1$ diffracted order into the incident beam and into higher diffracted orders.

Finally, the presence of guided modes is unavoidable in these systems. However, parameters can be chosen such that the guided modes are not resonant with the SPP, reducing their effects. Alternatively, for gratings localized in the waveguide core, the guided modes can act as a route for SPP–SPP interactions with energy coupled from SPP to guided modes, diffracted into higher order guided modes and finally coupled back into higher order SPP.

This analysis highlights the importance of the many control parameters involved in this system. The simplified equations are a powerful tool to study the response of the system to these parameters and provide the means to choose parameters such that the strongest possible SPP diffraction is observed.

ACKNOWLEDGMENTS

KRD and GD gratefully acknowledge Professor Nicholas Abbott and the Department of Chemical and Biological Engineering, University of Wisconsin–Madison, for their hospitality during the writing of this paper.

REFERENCES

1. A. V. Zayats, I. I. Smolyaninov, and A. A. Maradudin, "Nano-optics of surface plasmon polaritons," Phys. Rep. **408**, 131–314 (2005).
2. J. Homola, S. S. Yee, and G. Gauglitz, "Surface plasmon resonance sensors: review," Sens. Actuators B **54**, 3–15 (1999).
3. K. Kneipp, H. Kneipp, I. Itzkan, R. R. Dasari, and M. S. Feld, "Surface-enhanced Raman scattering and biophysics," J. Phys. Condens. Matter **14**, R597–R624 (2002).
4. S. A. Maier, P. G. Kik, H. A. Atwater, S. Meltzer, E. Harel, B. E. Koel, and A. A. G. Requicha, "Local detection of electromagnetic energy transport below the diffraction limit in metal nanoparticle plasmon waveguides," Nat. Mater. **2**, 229–232 (2003).
5. M. Malmqvist, "Biospecific interaction analysis using biosensor technology," Nature **361**, 186–187 (1993).
6. C. Holmes, K. R. Daly, I. J. G. Sparrow, J. C. Gates, G. D'Alessandro, and P. G. R. Smith, "Excitation of surface plasmons using tilted planar-waveguide Bragg gratings," IEEE Photon. J. **3**, 777–788 (2011).
7. W. L. Barnes, A. Dereux, and T. W. Ebbesen, "Surface plasmon subwavelength optics," Nature **424**, 824–830 (2003).
8. N. P. K. Cotter, T. W. Preist, and J. R. Sambles, "Scattering-matrix approach to multilayer diffraction," J. Opt. Soc. Am. A **12**, 1097–1103 (1995).
9. F. Yang and J. R. Sambles, "Optical fully leaky mode characterization of a standard liquid-crystal cell," J. Opt. Soc. Am. B **16**, 488–497 (1999).
10. M. E. Caldwell and E. M. Yeatman, "Surface-plasmon spatial light modulators based on liquid crystal, Appl. Opt. **31**, 3880–3891 (1992).
11. K. R. Welford and J. R. Sambles, "Detection of surface director reorientation in a nematic liquid crystal," Appl. Phys. Lett. **50**, 871–873 (1987).
12. K. R. Welford, J. R. Sambles, and M. G. Clark, "Guided modes and surface plasmon-polaritons observed with a nematic liquid crystal using attenuated total reflection," Liq. Cryst. **2**, 91–105 (1987).

13. D. W. Berreman, "Optics in stratified and anisotropic media: 4×4-matrix formulation," J. Opt. Soc. Am. B **62**, 502–510 (1972).
14. D. Y. K. Ko and J. R. Sambles, "Scattering matrix method for propagation of radiation in stratified media: attenuated total reflection studies of liquid crystals," J. Opt. Soc. Am. A **5**, 1863–1866 (1988).
15. E. N. Glytsis and T. K. Gaylord, "Three-dimensional (vector) rigorous coupled-wave analysis of anisotropic grating diffraction," J. Opt. Soc. Am. A **7**, 1399–1420 (1990).
16. M. Auslender and S. Hava, "Scattering-matrix propagation algorithm in full-vectorial optics of multilayer grating structure," Opt. Lett. **21**, 1765–1767 (1996).
17. S. B. Abbott, K. R. Daly, G. D'Alessandro, M. Kaczmarek, and D. C. Smith, "Photorefractive control of surface plasmon polaritons in a hybrid liquid crystal cell," Opt. Lett. **37**, 2436–2438 (2012).
18. S. B. Abbott, K. R. Daly, G. D'Alessandro, M. Kaczmarek, and D. C. Smith, "Hybrid liquid crystal photorefractuve system for the photorefractive coupling of surface plasmon polaritons," J. Opt. Soc. Am. B **29**, 1947–1958 (2012).
19. E. Kretschmann and H. Raether, "Radiative decay of non radiative surface plasmons excited by light," Z. Naturforsch. A **23**, 2135–2136 (1968).
20. M. Kaczmarek, A. Dyadyusha, S. Slussarenko, and I. C. Khoo, "The role of surface charge field in two-beam coupling in liquid crystal cells with photoconducting polymer layers," J. Appl. Phys. **96**, 2616–2623 (2004).
21. K. R. Daly, S. B. Abbott, G. D'Alessandro, D. C. Smith, and M. Kaczmarek, "Theory of hybrid photorefractive plasmonic liquid crystal cells," J. Opt. Soc. Am. B **28**, 1874–1881 (2011).
22. K. Okamoto, *Fundamentals of Optical Waveguides* (Academic, 2000).
23. J. J. Quinn and K. S Yi, *Solid State Physics* (Springer, 2009).
24. T. W. Preist, N. P. K. Cotter, and J. R. Sambles, "Periodic multilayer gratings of arbitrary shape," J. Opt. Soc. Am. A **12**, 1740–1748 (1995).
25. G. S. Garcia Quirino, J. J. Sanchez-Mondragon, and S. Stepanov, "Nonlinear surface optical waves in photorefractive crystals with a diffusion mechanism of nonlinearity," Phys. Rev. A **51**, 1571–1577 (1995).
26. L. M. Delves and J. N. Lyness, "A numerical method for locating the zeros of an analytic function," Math. Comput. **21**, 543–560 (1967).
27. E. Anemogiannis, E. N. Glytsis, and T. K. Gaylord, "Efficient solution of eigenvalue equations of optical wave guiding structures," J. Lightwave Technol. **12**, 2080–2084 (1994).
28. K. R. Daly, C. Holmes, J. C. Gates, P. G. R. Smith, and G. D'Alessandro, "Complete mode structure analysis of tilted Bragg grating refractometers in planar waveguides toward absolute index measurement," IEEE Photon. J. **3**, 861–871 (2011).
29. K. R. Daly, N. Podoliak, O. Buchnev, M. Kaczmarek, and G. D'Alessandro, "Optimal liquid crystal modulation controlled by surface alignment and anchoring strength," J. Opt. Soc. Am. B **29**, 2166–2175 (2012).
30. A. C. King, J. Billingham, and S. R. Otto, *Differential Equations: Linear, Nonlinear, Ordinary, Partial* (Cambridge University, 2003).
31. E.D. Palik, *Handbook of Optical Constants of Solids, Volumes I, II, and III: Subject Index and Contributor Index* (Academic, 1985).